Structure of ^{18}Ne and the breakout from the hot CNO cycle

K. I. Hahn,[1,*] A. García,[2,3] E. G. Adelberger,[2] P. V. Magnus,[2] A. D. Bacher,[4] N. Bateman,[1] G. P. A. Berg,[4]
J. C. Blackmon,[5,†] A. E. Champagne,[5,6] B. Davis,[3] A. J. Howard,[1] J. Liu,[4] B. Lund,[1] Z. Q. Mao,[7,‡] D. M. Markoff,[2]
P. D. Parker,[1] M. S. Smith,[1,†] E. J. Stephenson,[4] K. B. Swartz,[2] S. Utku,[1] R. B. Vogelaar,[7] and K. Yildiz[1]

[1]*Wright Nuclear Structure Laboratory, Yale University, New Haven, Connecticut 06520-8124*
[2]*Nuclear Physics Laboratory GL-10, University of Washington, Seattle, Washington 98195*
[3]*Department of Physics, University of Notre Dame, Notre Dame, Indiana 46556*
[4]*Indiana University Cyclotron Facility, Bloomington, Indiana 47408*
[5]*Department of Physics and Astronomy, University of North Carolina at Chapel Hill, Chapel Hill, North Carolina 27599*
[6]*Triangle Universities Nuclear Laboratory, Duke University, Durham, North Carolina 27706*
[7]*Department of Physics, Princeton University, Princeton, New Jersey 08544*

We used the ^{16}O(^{3}He,n)^{18}Ne, ^{12}C(^{12}C,^{6}He)^{18}Ne, and ^{20}Ne(p,t)^{18}Ne reactions to study ^{18}Ne states up to an excitation energy of 10 MeV, with emphasis on levels corresponding to ^{14}O(α,p)^{17}F and ^{17}F(p,γ)^{18}Ne resonances that could strongly affect these reaction rates in hot stellar environments. Excitation energies, widths, absolute cross sections, and angular distributions were measured. We found previously unidentified states at $E_x = 6.15\pm0.01$ MeV, 7.12 ± 0.02 MeV, 7.35 ± 0.02 MeV, 7.62 ± 0.02 MeV, 8.30 ± 0.02 MeV, (8.45 ± 0.03 MeV), 8.55 ± 0.03 MeV, 8.94 ± 0.02 MeV, and 9.58 ± 0.02 MeV. We combined level width, cross section, and angular distribution data to infer J^π values for a number of the new levels as well as for the previously known 5.1-MeV doublet. Using information from our experiments, we recalculated the ^{14}O(α,p) ^{17}F reaction rate, which constitutes a possible path out of the hot CNO cycle into the rp process and could play an important role in transforming nuclei involved in the hot CNO cycle into heavier nuclei with $Z \geq 10$. [S0556-2813(96)03709-0]

PACS number(s): 26.20.+f, 25.55.Hp, 27.20+n, 97.39.Qt

I. INTRODUCTION

The ^{14}O(α,p)^{17}F and ^{17}F(p,γ)^{18}Ne reactions play crucial roles in the advanced stages of astrophysical hydrogen burning. The ^{14}O(α,p)^{17}F(p,γ)^{18}Ne($\beta^+\nu$)^{18}F(p,α)^{15}O reaction sequence can provide a path around the relatively slow positron decay of ^{14}O in the hot CNO cycle, while the reaction sequence ^{14}O(α,p)^{17}F(p,γ)^{18}Ne($\beta^+\nu$)^{18}F(p,γ)^{19}Ne can provide an alternate path from the hot CNO cycle to the rapid proton burning (rp) process. The energy release in the hot CNO cycle is limited by the decay rate of ^{14}O($t_{1/2}=70.6$ s) and ^{15}O($t_{1/2}=122$ s). Wallace and Woosley [1] have shown that at sufficiently high temperatures and densities α capture on ^{14}O and ^{15}O competes favorably with β decay. This breaks the hot CNO cycle and makes the transition into the rp process where the energy generation rate can increase by two orders of magnitude.

The ^{14}O(α,p)^{17}F and ^{17}F(p,γ)^{18}Ne reaction rates depend sensitively on the excitation energies, spins, and partial and total widths of the relevant resonances in ^{18}Ne. For example, a previous [2] study of the ^{16}O(^{3}He,n)^{18}Ne reaction found that the missing 3^+ level lies ~ 230 keV higher than

calculated by Wiescher, Görres, and Thielemann [3]; this caused its contribution to the ^{17}F(p,γ) reaction rate to be about two orders of magnitude smaller than they had predicted.

Two calculations [4,5] of the ^{14}O(α,p)^{17}F reaction rate have recently appeared. These studies were necessarily based largely on theoretical expectations as experimental information about the level structure of ^{18}Ne at $E_x>5$ MeV was very sparse. In fact, the summary of previous experimental results [2,6] for ^{18}Ne and ^{18}O displayed in Fig. 1 shows that the ^{18}Ne analogs of a number of ^{18}O levels in the region $E_x>5$ MeV were yet undiscovered. Because these could have a large effect on the predicted ^{17}F(p,γ)^{18}Ne and ^{14}O(α,p)^{17}F reaction rates, we have investigated the structure of ^{18}Ne at high excitation energies. We describe our studies of the ^{16}O(^{3}He,n)^{18}Ne, ^{12}C(^{12}C,^{6}He)^{18}Ne, and ^{20}Ne(p,t)^{18}Ne reactions in Secs. II, III, and IV, respectively. These results are analyzed to yield information on the structure of ^{18}Ne in Sec. V. This information is then used to recalculate the ^{14}O(α,p)^{17}F reaction rate in Sec. VI.

II. ^{16}O(^{3}He,n)^{18}Ne REACTION

A. Experimental setup

The ^{16}O(^{3}He,n)^{18}Ne studies were made using the pulsed-beam time-of-flight spectrometer at the University of Washington tandem accelerator. Details of this facility are given in Refs. [2,7,8]. For this work, we used a set of three unshielded 12.7-cm-diam liquid-scintillation detectors. Two of these BC-501 scintillators were 5.1 cm thick and the third

_____

*Present address: RIKEN (Institute of Physical and Chemical Research), Hirosawa, Wako, Saitama 351-01, Japan.

†Present address: Physics Division, Oak Ridge National Laboratory, Oak Ridge, TN 37831-6354.

‡Present address: Department of Physics, University of Pennsylvania, Philadelphia, PA 19104.
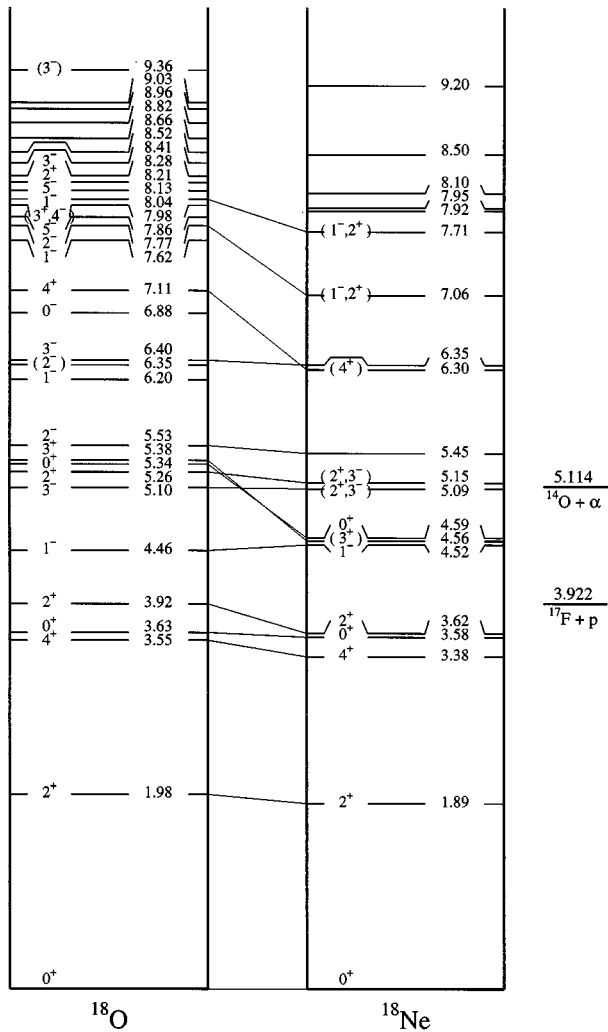
FIG. 1. Previous level diagrams of ^{18}O and ^{18}Ne from Ref. [6] including the 4.56-MeV state in ^{18}Ne from Ref. [2].

2.5 cm thick; all had excellent neutron-gamma discrimination capabilities. The efficiencies of our detectors as functions of neutron energy were determined using the ^{7}Li(p,n) reaction, for which the absolute cross section is well known [9,10].

The oxygen targets were prepared by anodizing high-purity Ta blanks in 0.1N sulfuric acid [11]. The resulting Ta$_2$O$_5$ layers had thicknesses of approximately 150 μg/ cm^2. The targets were mounted in a clean cryo-pumped chamber operating at pressures below 5×10^{-7} Torr. To avoid any residual C buildup, we moved the target periodically so that the beam again struck a "fresh" surface. The only detectable contaminant in our spectra was ^{12}C. Its effect on our spectra was determined by always taking data with a C target under the same conditions as the ^{16}O(^{3}He,n) ^{18}Ne data.

B. Results

Choosing the best beam energy to study a particular level with the (^{3}He,n) reaction involves a trade-off between good energy resolution (which implies lower beam energies) and appreciable cross section for populating the level (which usually implies higher beam energies). Figure 2 shows a
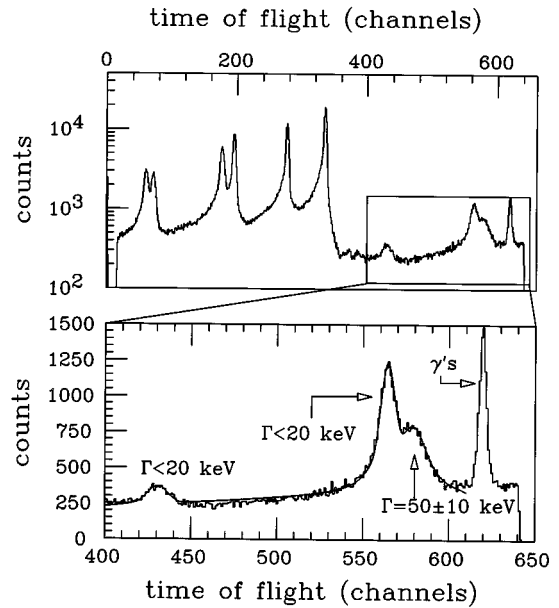

FIG. 2. Time-of-flight spectrum showing the 5.1-MeV doublet and 5.4-MeV level in ^{18}Ne. This was taken at $\theta_n=0°$, $E_{3\mathrm{He}}=10.90$ MeV, and a flight path of 4.53 m. The expanded region of the spectrum covers the region of very slow "wrap-around" neutrons (i.e., neutrons whose flight times exceeded the beam burst repetition period). The peak labeled "γ" is a small residue of the intense prompt γ flash.

time-of-flight spectrum taken at $E_{3\mathrm{He}}=10.9$ MeV; the smooth curve is a fit obtained using the procedure explained in Ref. [2]. This spectrum was used to extract energies and widths of the ^{18}Ne doublet at $E_x\approx5.1$ MeV and of the level at $E_x=5.45$ MeV. The extracted values are shown in Table I.

Figure 3 shows a 0° neutron time-of-flight spectrum taken at $E_{3\mathrm{He}}=14.0$ MeV to study energy levels at higher excitation in ^{18}Ne. Several previously unobserved levels were seen. We obtained an angular distribution at $E_{3\mathrm{He}}=14.5$ MeV in order to (1) confirm that the new levels belonged to ^{18}Ne and not to another nucleus produced via a target contaminant, by observing the kinematic behavior of the corresponding peaks, and (2) extract spin and parity information about these levels by comparing the measured angular distribution to distorted-wave Born approximation (DWBA) calculations.

Figure 4 displays time-of-flight data obtained at seven different neutron angles. The data, transformed into excitation energy spectra, show previously unobserved levels at $E_x=6.15\pm0.01$ MeV and 7.35 ± 0.02 MeV, and an apparent doublet at $E_x\approx7.07$ MeV (see Table I). In order to facilitate normalization we fixed one of our three neutron counters at zero degrees and moved the other two to laboratory angles of 11°, 23°, 34°, 47°, 64°, and 79°. The data were fitted using the program described in Ref. [2], with the constraint that the level widths and excitation energies be identical in all spectra. The program included an exponential tail in the detector resolution function to account for neutron scattering by matter close to the target or detector. These tails were assumed to be a function of the detector only. Note, however, that, in contrast to the situation of the lower excitation energy levels, there is a now background contribution from three- and four-body reactions, especially ^{16}O(^{3}He,np)^{17}F, which has a

TABLE I. ^{18}Ne levels with $E_x \geq 5$ MeV observed in ^{16}O(^{3}He,n)^{18}Ne.

This work		Previous results[a]		
E_x (MeV$\pm$keV)	Γ (keV)	E_x (MeV$\pm$keV)	J^π	Γ (keV)
5.106 ± 8	50 ± 10	5.090 ± 8	$(2^+,3^-)$	40 ± 20
5.153 ± 8	≤20	5.146 ± 7	$(2^+,3^-)$	25 ± 15
5.454 ± 8	≤20	5.453 ± 10	(2^-)	≤50
6.15 ± 10	≤40			
6.30 ± 10		6.297 ± 10		≤60
6.35 ± 10		6.353 ± 10		≤60
7.07 ± 10[b]	200 ± 40	7.062 ± 12		180 ± 50
(7.05 ± 30)[b]	(≤120)			
(7.12 ± 30)[b]	(≤120)			
7.35 ± 18	≤50			
7.72 ± 10	≤30	7.713 ± 10		≤50
		7.915 ± 10		≤50
7.94 ± 10	40 ± 10	7.949 ± 10		≤60
8.11 ± 10	≤30	8.10 ± 14		≤50
		8.50 ± 30		≤120
		9.20 ± 10		≤50

[a]Reference [6].

[b]We fitted our spectra with either one level at $E_x = 7.07$ MeV and $\Gamma = 200$ keV or the doublet indicated in parentheses. For this last case we consistently found a smaller χ^2 per degree of freedom.

threshold at a ^{18}Ne excitation energy of 3.922 MeV.

Angular distributions of the observed neutron groups are plotted in Fig. 5, along with DWBA calculations performed with the code DWUCK4 [12] using the parameters of Ref. [13]. Our measurements of E_n as a function of θ_n demonstrated that all the observed groups did arise from the ^{16}O(^{3}He,n)^{18}Ne reaction. However, the angular distributions of the higher-lying levels generally do not exhibit any clear structures that could be used to extract the transferred orbital angular momentum. The top two panels show the ground state and first excited state that are clearly resolved in our spectra (see Fig. 3) and whose L values are known. The reasonable agreement of the observed and calculated distributions supports our parameter set. Note that the angular
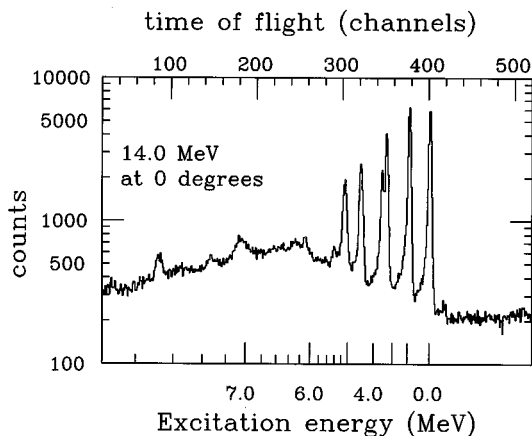

FIG. 3. Neutron time-of-flight spectrum at $E_{^3\mathrm{He}} = 14$ MeV, $\theta_n = 0°$, and a flight path of 4.53 m.

distribution for the $E_x = 5.45$ MeV level ($J^\pi = 2^-$) is not forward peaked, which is consistent with its being an unnatural-parity level.

III. ^{12}C(^{12}C,^{6}He)^{18}Ne REACTION

A. Introduction

Almost all previous experimental studies of ^{18}Ne were done using the ^{16}O(^{3}He,n) and ^{20}Ne(p,t) reactions. These are dominated by a direct two-nucleon transfer mechanism and so preferentially populate only natural-parity states in ^{18}Ne. We, therefore, also investigated the ^{12}C(^{12}C,^{6}He) reaction [14], which proceeds primarily by a compound nuclear mechanism. This reaction is not particularly selective and can populate all but the $J^\pi = 0^-$ states of ^{18}Ne. Our results are discussed and compared to statistical model calculations below.

B. Experimental setup

A 30–300-pnA beam of 80-MeV ^{12}C ions from the Yale ESTU tandem accelerator bombarded natural carbon targets with thicknesses between 20 and 50 μg/cm^2. The ^{12}C+^{12}C reaction products at laboratory angles of 1°, 2°, 4°, 6°, 7°, and 10° were analyzed in an Enge split-pole spectrograph. The spectrograph focal-plane detector consisted of a gas proportional counter and a plastic scintillator [14]. The isobutane-filled proportional counter had a cathode that measured the energy loss in the gas, ΔE, and two position-sensitive wires separated by 10 cm. Each of these wires was surrounded by a series of small copper split rings with a 2.5-mm segmentation that served as tapped-delay-line pickups connected to lumped delay-line chips. The relative delay between the signals at the two ends of a wire determined the rigidity of the particle, ρ. After passing through the gas volume, most particles stopped in a 6.4-mm-thick BC-404 plastic scintillator that determined the residual energy E.

For measuring absolute cross sections, we used both a Faraday cup and a silicon surface-barrier detector. The surface-barrier detector, located at 40° in the target chamber, was used to calibrate the Faraday cup and normalize the beam current integrator readings from the Faraday cup at various angles. The 2°, 4°, 6°, 7°, and 10° data were taken using a Faraday cup located in the target chamber. This Faraday cup was removed for the 1° run and replaced by a beam stop located on the focal plane.

C. Data analysis and results

Because the ^{12}C+^{12}C reaction produces about 10^5 times more α particles than ^{6}He particles it would be difficult to separate the ^{6}He group cleanly from the α group with conventional $\Delta E \otimes E$ particle identification techniques. The spectrometer provided an additional parameter of particle momentum that was used to help separate and identify the various particle groups. The ^{6}He group was identified by three 2-dimensional gates placed on the parameters, ΔE, E, and ρ.

Because we used natural carbon targets, we expected some contributions from the ^{13}C(^{12}C,^{6}He)^{19}Ne reaction; these were determined by running with a ^{13}C target in the
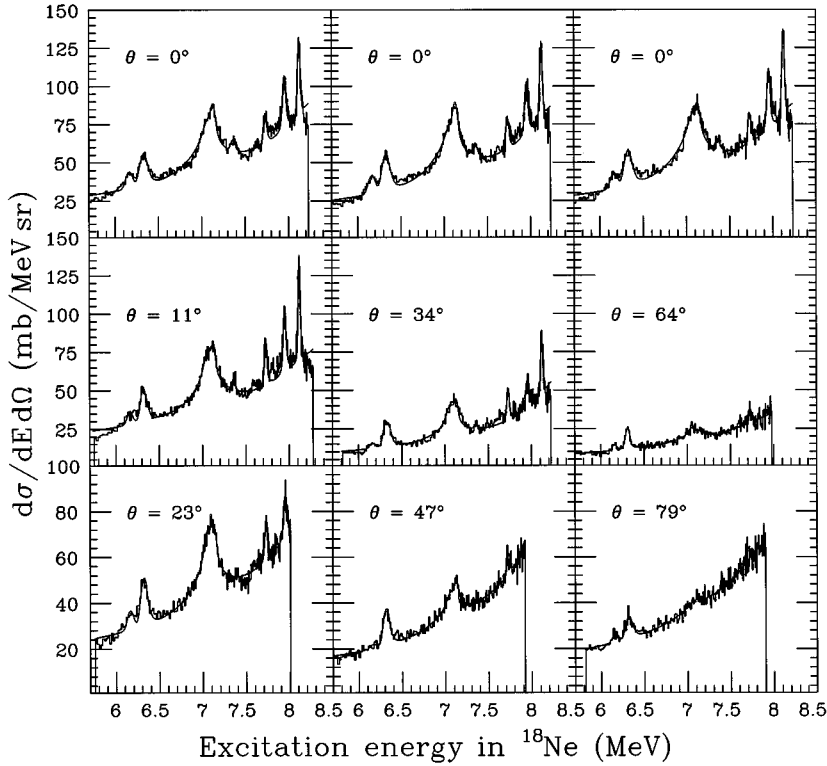
FIG. 4. ''Excitation energy'' spectra taken at different angles and $E_{^3\text{He}}=14.5$ MeV. The fits were obtained using identical level parameters at each angle and letting the program fit the area.

FIG. 5. ^{16}O(^{3}He,n) angular distributions taken at $E_{^3\text{He}}=14.5$ MeV. The lines show DWBA calculations for different values of the transferred orbital angular momentum; solid line, $L=0$; dashed line, $L=1$; dotted line, $L=2$; dot-dashed line, $L=3$; solid line, $L=4$.

middle of each of the natural carbon target runs, without changing any experimental conditions or parameters. The ^{6}He spectra at 4° obtained with natural carbon and ^{13}C targets are shown in Fig. 6. No evidence of other contaminants was observed.

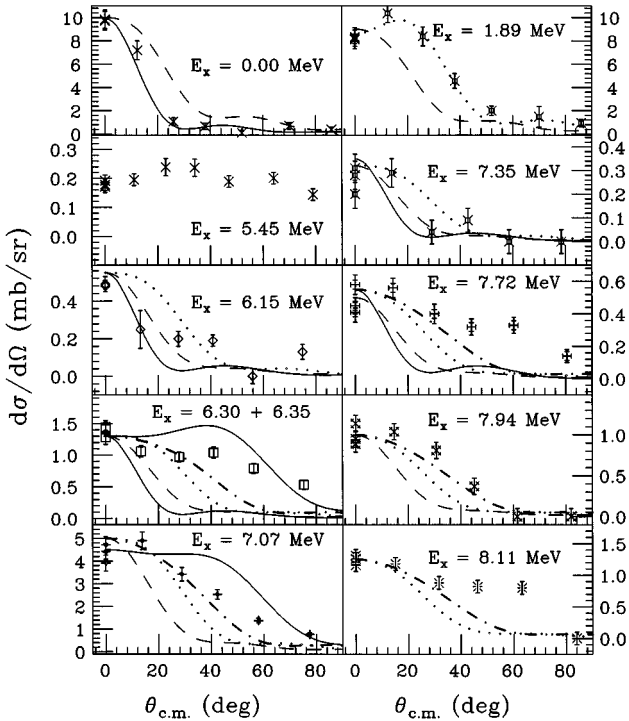The ^{12}C(^{12}C,^{6}He)^{18}Ne spectra were quite clean even though the strongest states had cross sections of only ~ 1 μb/sr. Data were obtained at six angles in the interval $1° \leqslant \theta_{\text{lab}} \leqslant 10°$ (Fig. 7) to measure the kinematic shifts of each ^{6}He group and test that it did arise from the ^{12}C(^{12}C, ^{6}He)^{18}Ne reaction, and to compare the resulting angular distributions with statistical-model compound-nucleus calculations discussed in Sec. III D below.

Several previously unobserved ^{18}Ne levels were seen (see Table II): states at $E_x=6.15$ MeV and $E_x=7.35$ MeV that confirm the ^{16}O(^{3}He,n) ^{18}Ne results in Sec. II, as well as new states at $E_x=7.12$ MeV, 7.62 MeV, 8.30 MeV, 8.55 MeV, 8.94 MeV, 9.58 MeV, and possibly 8.45 MeV (only observed at two angles).

D. Angular distributions

Figure 7 shows ^{6}He spectra obtained at six angles. For the 1° run, it was necessary to put a 0.125-mm-thick Al foil in front of the gas detector to stop the ^{12}C^{4+} particles (from a small fraction of ^{12}C^{5+} projectiles that picked up an electron in the target) with the same rigidity as the ^{6}He particles corresponding to 3.5–4.5-MeV states of ^{18}Ne. Although the absorber was thick enough to stop the ^{12}C projectiles, their interactions in the foil produced light particles that entered the detector and produced the background in the $3.5 < E_x < 4.5$ MeV region of ^{18}Ne seen in the 1° spectrum shown in Fig. 7. Multiple scattering in the absorber reduced the position resolution for the ^{6}He particles in the 1° run, resulting in an energy resolution of ~ 100 keV, compared to ~ 70 keV at other angles.

The ^{12}C(^{12}C,^{6}He)^{18}Ne reaction is expected to take place, at the 80-MeV ^{12}C beam, via a mechanism in which the compound nucleus decays to various channels with relative strengths that can be predicted via a statistical-model calcu-
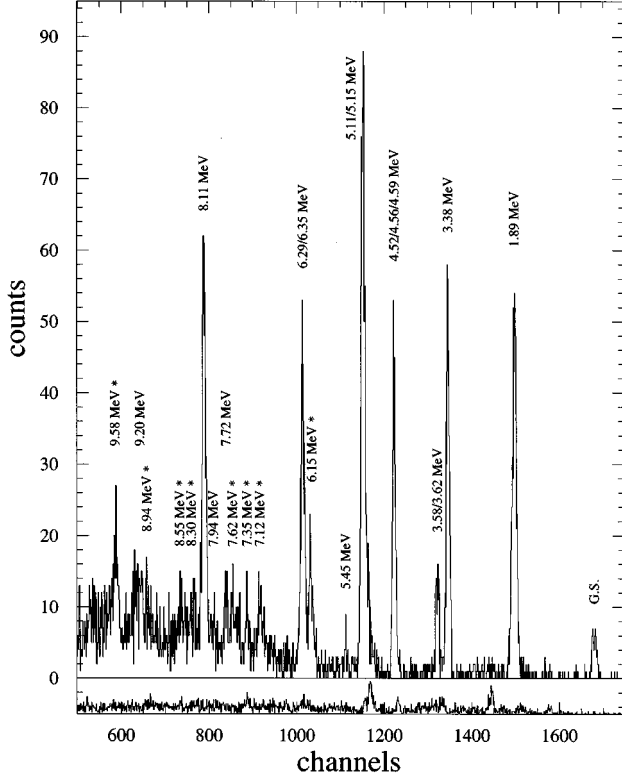
FIG. 6. Position spectrum from the ^{12}C(^{12}C, ^{6}He)^{18}Ne experiment. Top: natural carbon target at 4°. Bottom: ^{13}C target. The asterisks indicate previously unobserved levels.
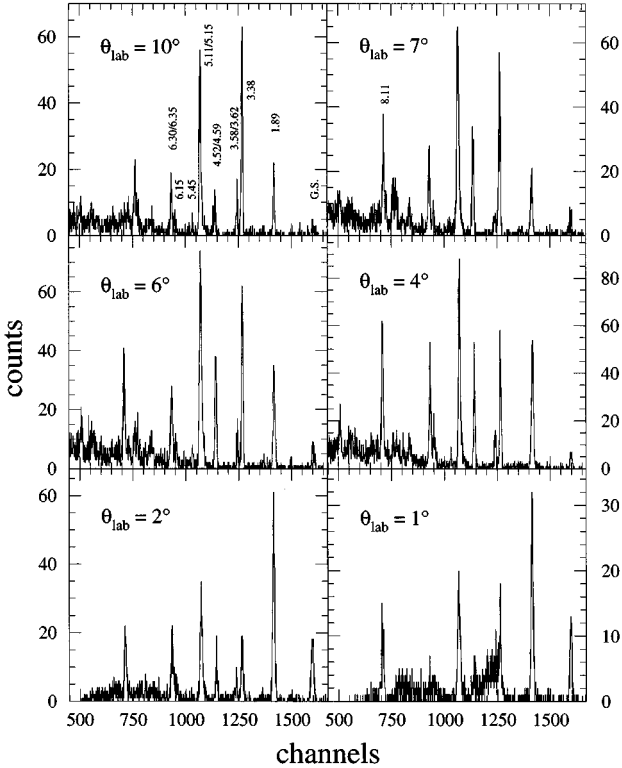

FIG. 7. ^{12}C(^{12}C,^{6}He)^{18}Ne position spectra taken at several angles with $E_{\text{lab}} = 80.0$ MeV.

TABLE II. ^{18}Ne levels with $E_x \geqslant 6$ MeV observed in ^{12}C(^{12}C, ^{6}He)^{18}Ne.

$\Theta = 4°$	$\Theta = 6°$	Weighted average value[a]
E_x (MeV$\pm$keV)	E_x (MeV$\pm$keV)	E_x (MeV$\pm$keV)
6.149$\pm$20	6.148$\pm$20	6.15$\pm$20
6.30[b]	6.30[b]	
7.122$\pm$20	7.108$\pm$30	7.12$\pm$20
7.353$\pm$20	7.363$\pm$30	7.35$\pm$20
7.618$\pm$20	7.630$\pm$20	7.62$\pm$20
7.733$\pm$20	7.732$\pm$20	7.73$\pm$20
7.940$\pm$30	7.948$\pm$20	7.94$\pm$20
8.11[c]	8.11[c]	
8.295$\pm$20	8.311$\pm$20	8.30$\pm$20
(8.451$\pm$30)	(8.445$\pm$30)	(8.45$\pm$30)
8.535$\pm$20	8.574$\pm$30	8.55$\pm$30
8.943$\pm$20	8.947$\pm$20	8.94$\pm$20
9.199$\pm$20	9.170$\pm$20	9.18$\pm$20
9.593$\pm$20	9.571$\pm$20	9.58$\pm$20

[a]Includes values from the other angles 2°, 7°, and 10°.
[b]The 6.30/6.35-MeV doublet could not be resolved. Because the calibration favored 6.30 MeV as explained in the text, this number was used for the calibration along with 0.00-, 1.89-, 3.38-, 5.45-, and 8.11-MeV states.
[c]Used for the calibration.

lation [15]. We used the computer code STATIS [16] to calculate the compound-nucleus cross sections for the ^{12}C(^{12}C, ^{6}He) reaction populating the various states in ^{18}Ne. The optical-model parameters used to calculate the transmission coefficients are listed in Table III.

Figure 8 compares the measured cross sections and the statistical-model calculations for some of the states in ^{18}Ne. The statistical model reproduces expected trends in the data. Note that the angular distribution for the $E_x = 5.45$ MeV level ($J^\pi = 2^-$) is not forward peaked, which is consistent with its being an unnatural-parity level. The angular distributions for the other ^{18}Ne levels did not present clear structures that could be used to extract reliable spin values.

IV. ^{20}Ne(p,t) ^{18}Ne REACTION

A. Introduction

We used the ^{20}Ne(p,t) ^{18}Ne reaction to study the higher excitation energy region of ^{18}Ne with better resolution

TABLE III. Optical-model parameters used in the analysis of the ^{12}C(^{12}C, ^{6}He) data.

Channel	V_{real} (MeV)	V_{imag} (MeV)	R_{real} (fm)	a_{real} (fm)	R_{imag} (fm)	a_{imag} (fm)	R_{Coulomb} (fm)
^{18}Ne + ^{6}He[a]	14.0	0.82[b]	6.18	0.35	6.41	0.56	6.0
^{20}Ne + α[a]	50.0	2.0[b]	4.94	0.59	4.94	0.46	3.92
^{23}Mg + n[a]	48.2	11.5[c]	3.56	0.65	3.55	0.47	0.0
^{23}Na + p[a]	56.0	13.5[c]	3.56	0.65	3.56	0.47	3.66
^{12}C + ^{12}C[d]	52.2	9.8[c]	4.76	0.53	4.76	0.53	3.92

[a]Reference [17].
[b]Surface absorption potential.
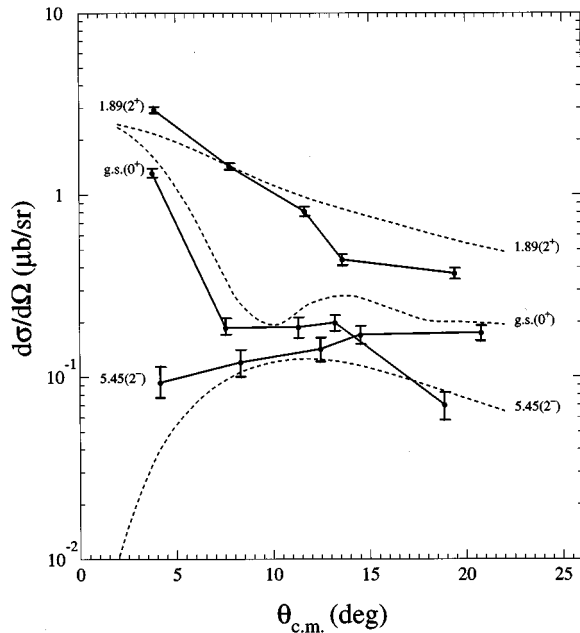[c]Volume absorption potential.
[d]Reference [18].

FIG. 8. Absolute Hauser-Feshbach statistical-model calculations compared to experimental angular distributions for ^{18}Ne states populated in the ^{12}C(^{12}C,^{6}He)^{18}Ne reaction at $E_{lab}=80.0$ MeV. The solid lines indicate experimental values; the dashed lines are model calculations.

than was possible in the ^{16}O(^{3}He,n)^{18}Ne and ^{12}C(^{12}C,^{6}He)^{18}Ne work, and to confirm, if possible, the previous observation [2] of the 3^+ state at 4.561 MeV. The keys to our measurements were implanted ^{20}Ne targets and the high-resolution magnetic spectrometers at the Indiana University Cyclotron Facility (IUCF) and at the Princeton University AVF cyclotron. The targets, consisting of ~7 μg/cm^2 of ^{20}Ne implanted into 40 μg/cm^2 carbon foils [19], allowed us to use dispersion matching techniques that would not have been possible with an extended gas target. The IUCF and Princeton results are discussed separately in the following sections.

B. Indiana experiment

1. Experimental setup

Data were taken with a 88.4-MeV proton beam with an average intensity of 130 nA. Measurements were made at laboratory angles of 6° and 11° using the high-resolution K600 spectrometer and its associated focal-plane detectors [20]. The focal-plane detector [20] consisted of two vertical drift chambers and two plastic scintillators located immediately after the chambers. The scintillator thicknesses were chosen so that the tritons from the ^{20}Ne(p,t)^{18}Ne reaction passed through the first scintillator and stopped in the second. This allowed us to separate the tritons cleanly from deuterons generated via the ^{20}Ne(p,d)^{19}Ne reaction. Dispersion matching was used to optimize the position resolution. For the 6° run the dispersion was matched using the intense proton group from the ^{12}C(p,p)^{12}C(g.s.) reaction at 7° which had the same kinematic factor ($k=1/p$ $dp/d\theta$) as the ^{20}Ne(p,t)^{18}Ne reaction at 6°. For the 11° run ($k=0.024$),

we interpolated the settings between the 6° ($k=0.012$) values and those appropriate for ^{12}C(p,p)^{12}C at 23° ($k=0.036$).

2. Data analysis and results

It was impossible to focus a wide range of ^{18}Ne states on the focal-plane detector because the focal surface was slightly curved and we used a large solid angle of 3.98 msr. However, with the angle as well as position information it was possible to make corrections and recover optimum performance at all positions without losing statistics. After corrections, we obtained an energy resolution of 20–25 keV for the ^{18}Ne levels of interest. (See Ref. [14] for a detailed description of the data-processing procedure.)

The final corrected triton position spectrum measured at 11° is shown in Fig. 9. All the peaks are identified as states of ^{18}Ne or of ^{11}C, ^{10}C, ^{14}O, and ^{26}Si from the ^{20}Ne(p,t)^{18}Ne, ^{13}C(p,t)^{11}C, ^{12}C(p,t)^{10}C, ^{16}O(p,t)^{14}O, and ^{28}Si(p,t)^{26}Si reactions, respectively. The origin of satellite peaks around the intense peaks from the ground and 3.353-MeV states of ^{10}C was never conclusively identified [21].

Figure 10 shows the energy region of $4.0<E_x<6.5$ MeV. We saw no indication of the 3^+ state in the middle of the 4.5-MeV doublet or in the $4.60<E_x<5.10$ MeV region; we could not investigate the region below $E_x<4.52$ MeV due to the intense ^{10}C ground state. We observed three levels, at 6.29, 6.35 MeV, and 7.92 MeV, in the energy range of $E_x \gtrsim 6.0$ MeV; all of these were also seen in the ^{16}O(^{3}He,n)^{18}Ne and ^{12}C(^{12}C,^{6}He)^{18}Ne reactions. The results of this experiment are listed in Table IV and are discussed in Sec. V.

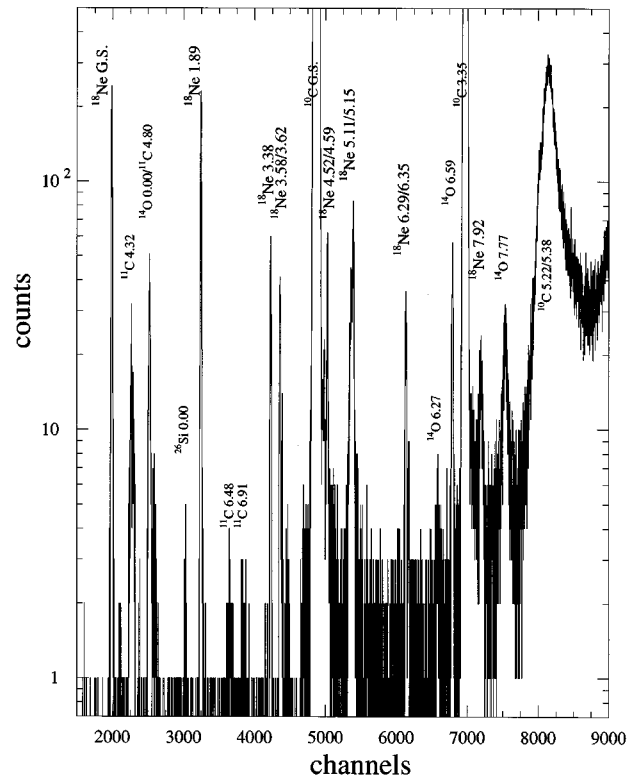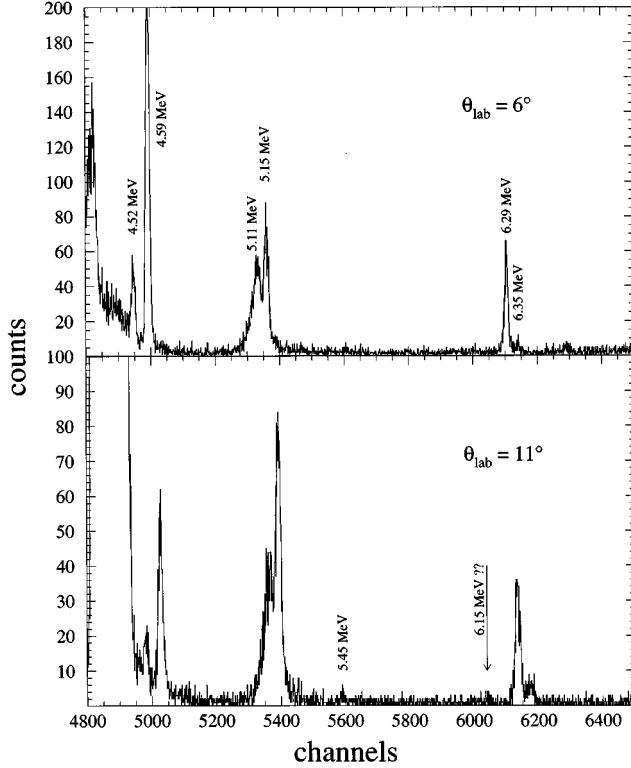FIG. 9. Position spectrum from the Indiana ^{20}Ne(p,t)^{18}Ne experiment at $\theta_t=11°$.

FIG. 10. Position spectra from the Indiana ^{20}Ne(p,t) experiment showing the $4.0 < E_x < 6.8$ MeV region of ^{18}Ne, taken at $\theta_t = 6°$ and $11°$. The arrow in the $11°$ spectrum shows where the 6.15-MeV level, which was seen in the ^{16}O$(^3$He$,n)$ and ^{12}C$(^{12}$C, ^{6}He) reactions, should lie.
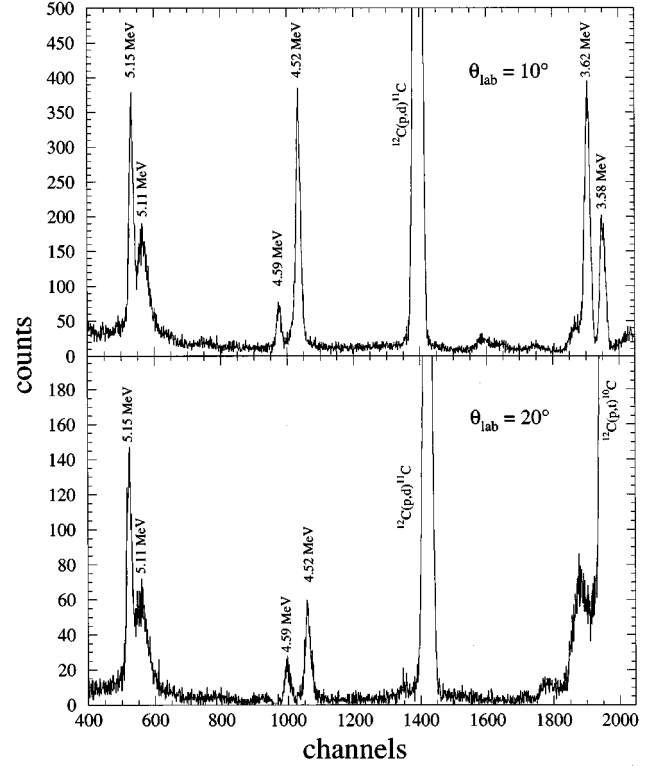

FIG. 11. Position spectra from the Princeton ^{20}Ne(p,t) experiment, showing the $3.0 < E_x < 6.0$ MeV region of ^{18}Ne, taken at $\theta_t = 10°$ and $20°$.

C. Princeton Experiment

1. Introduction

At the maximum proton energy for the Princeton AVF cyclotron, ~ 44 MeV, we were not able to study ^{18}Ne levels with $E_x \geq 6.0$ MeV because at this energy the elastic protons have the same magnetic rigidity as the tritons of interest. Therefore, we were restricted to studying ^{18}Ne states below 6.0 MeV.

2. Experimental setup

We studied the ^{20}Ne(p,t) ^{18}Ne reaction at $E_p = 40$ MeV and $\theta_{lab} = 10°$ and $20°$ using a QDDD spectrograph [22]. Although the large dispersion of the spectrograph limited the range of energies that could be examined at any one setting

of the magnetic field, we were able to study the ^{18}Ne level structure from 3.5 MeV to 5.3 MeV with one magnet setting.

The focal-plane detector consisted of two position-sensitive resistive-wire gas proportional counters that measured the position and the rate of the energy loss of the incident ions and a 6.4-mm-thick scintillator that measured the residual energy. Signals from these detectors were used to determine the momentum and the identity of particles.

3. Data analysis and results

Figure 11 shows the triton position spectra measured at $10°$ and $20°$, which have an energy resolution of ≈ 15 keV. These spectra show the previously known ^{18}Ne states, but give no evidence for new levels such as the 4.56-MeV level, seen in the ^{16}O$(^3$He$,n)$ reaction between the two established levels at 4.5 MeV. The measured widths of the 5.11/5.15-MeV doublet are listed in Table V.

V. STRUCTURE OF ^{18}Ne

Our studies of ^{18}Ne using the ^{16}O$(^3$He$,n)$, ^{12}C$(^{12}$C, ^{6}He), and ^{20}Ne(p,t) reactions discussed in Secs. II (including Ref. [2]), III, and IV, respectively, have yielded new information on the level structure of ^{18}Ne above the ^{17}F + p and ^{14}O + α thresholds ($E_x > 4.0$ MeV). These new results are summarized below and in Fig. 12 and Table V.

A. "Missing" 3^+ state

This state is expected to provide a strong $\ell = 0$ resonance in the ^{17}F + p channel which, depending on its resonant

TABLE IV. ^{18}Ne states seen in the Indiana experiment.

$\Theta = 6°$		$\Theta = 11°$	
E_x (MeV±keV)	Γ (keV)	E_x (MeV±keV)	Γ (keV)
5.095[a]	49±6	5.095[a]	49±6
5.150[a]	≤20	5.150[a]	≤20
6.286±10	≤20	6.286±10	≤20
6.343±20		6.346±10	45±10
7.924±20	70±20	7.920±20	70±20

[a]These states together with the seven lowest ^{18}Ne states were used for the energy calibration.

TABLE V. Summary of ^{18}Ne states with $E_x \geq 4$ MeV.

^{16}O(^{3}He,n)^{18}Ne		^{12}C(^{12}C,^{6}He)^{18}Ne[a]	^{20}Ne(p,t)^{18}Ne[b]		J^π
E_x (MeV±keV)	Γ (keV)	E_x (MeV±keV)	E_x (MeV±keV)	Γ (keV)	
4.520±7	9±6		4.520[c]		$1^{-\,\mathrm{d}}$
4.561±9	25[e]				3^+
4.589±7	4±4		4.589[c]		$0^{+\,\mathrm{d}}$
5.106±8	50±10		5.106[c]	49±6; 45±5[f]	2^+
5.153±8	≤20		5.153[c]	≤20; ≤15[f]	3^-
5.454±8	≤20	5.45[g]			2^-
6.15±10	≤40	6.15±20			(1^-)
6.30±10			6.286±10	≤20	(3^-)
6.35±10			6.345±10	45±10	(2^-)
7.07±10	200±40				
(7.05±30)	(≤120)				(4^+)
(7.12±30)	(≤120)	7.12±20			
7.35±18	≤50	7.35±20			(1^-)
		7.62±20			
7.72±10	≤30	7.73±20			
7.94±10	40±10	7.94±20	7.92±20	70±20	
8.11±10	≤30	8.11[g]			
		8.30±20			
		(8.45±30)			
		8.55±30			
		8.94±20			
		9.18±20			
		9.58±20			

[a]The multiplets at $E_x = 4.5$, 5.1, and 6.3 MeV are not resolved in the ^{12}C(^{12}C,^{6}He)^{18}Ne data.
[b]From the Indiana experiment unless specified otherwise.
[c]From our ^{16}O(^{3}He,n)^{18}Ne experiment.
[d]From Ref. [6].
[e]Estimated from a Woods-Saxon calculation.
[f]From the Princeton experiment.
[g]Used for the energy calibrations.

energy and partial widths, could greatly influence the thermonuclear reaction rate of this channel. The only experimental evidence of this 3^+ state has been found in the ^{16}O(^{3}He,n)^{18}Ne reaction, where a level in the middle of the 4.5-MeV doublet was observed in a single high-resolution spectrum at a backward angle ($\theta_{\mathrm{lab}} = 124.7°$) [2]. Although we did not see any evidence of this state in ^{20}Ne(p,t)^{18}Ne measurements at forward angles, this is not surprising as a 3^+ level cannot be populated in the direct two-nucleon transfer process that dominates the (p,t) reaction at forward angles, and was only seen in ^{16}O(^{3}He,n)^{18}Ne under kinematic conditions that strongly *inhibit* direct processes (backward angles and low neutron energies). The relatively poor resolution of our ^{12}C(^{12}C,^{6}He) study prevented us from seeing a level in the middle of the 4.5-MeV doublet. However, the fact that no new levels were seen in the excitation region from 4 to 5 MeV provides indirect, albeit weak, support for the (^{3}He,n) result.

B. 5.1-MeV doublet

Based on energy considerations and ^{16}O(^{3}He,n)^{18}Ne strengths, the 5.11- and 5.15-MeV levels of ^{18}Ne are expected to correspond to the 5.10-MeV ($J^\pi = 3^-$) and 5.25-MeV ($J^\pi = 2^+$) levels of ^{18}O, although it is not obvious which ^{18}Ne level is 3^- and which is 2^+. Wiescher *et al.* [4] assigned 3^- to the 5.11-MeV level and 2^+ to the 5.15-MeV level on the basis of calculated Thomas-Ehrman shifts of the mirror ^{18}O and ^{18}Ne levels. Funck *et al.* [5] used a microscopic multichannel calculation to arrive at the same doublet spin assignments as Wiescher *et al.*

However, the two levels of the 5-MeV ^{18}Ne doublet lie so close together that calculated level *shifts* cannot give a reliable assignment of the spins. On the other hand, the *widths* of the two levels, $\Gamma(5.11) = 45 \pm 5$ keV and $\Gamma(5.15) \leq 15$ keV, are very different, and these widths can be used to discriminate reliably between the two possible spin assignments [7], and provide strong evidence that the previous spin assignments of Refs. [4,5] should be reversed.

As a result of penetrability considerations, a level emitting protons with low ℓ values will generally have a larger width than a state which must emit protons with a higher ℓ. We placed this argument on a quantitative footing by Woods-Saxon calculations of the Coulomb energy shifts and widths of a 2^+ state ($s_{1/2}d_{5/2}$ configuration) and a 3^- state (either $[d_{5/2}]^3[p_{1/2}]^{-1}$ or $d_{5/2}f_{7/2}$ configurations) as outlined below and in the Appendix.
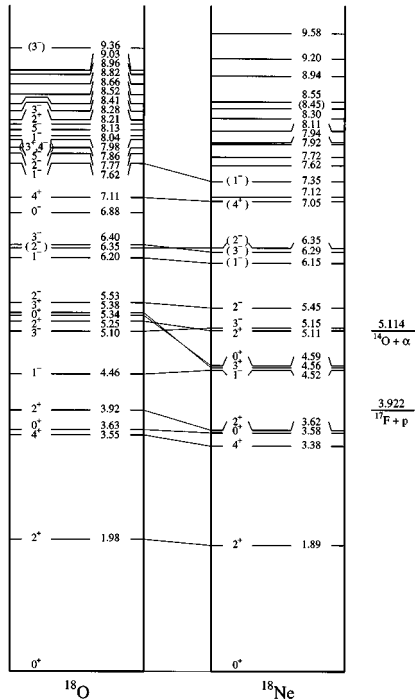
FIG. 12. Level diagrams of ^{18}O and ^{18}Ne including results from this work, Ref. [2], Ref. [23], and accepted values from Ref. [6].

The Thomas-Ehrman shift of the 2^+ state was estimated by finding the Woods-Saxon potential ($V=47.5$ MeV) that placed the 2^+ level in ^{18}O at its observed energy $E_x=5.25$ MeV. We then used this potential plus the added Coulomb interaction to predict the excitation energy of the corresponding 2^+ state in ^{18}Ne. This gave a Thomas-Ehrman energy shift $\triangle E=-0.83$ MeV for a pure single-particle case. Multiplying this energy shift by the ^{17}O(d,p) ^{18}O spectroscopic factor [24] of the analog level, $S(s_{1/2}) = 0.35\pm0.09$, we predict an excitation energy $E_x(^{18}$Ne$)=E_x(^{18}$O$) +\triangle E\times S=5.0$ MeV which is close to the actual excitation energy of either member of the 5.1-MeV doublet.

The expected width of the 2^+ ^{18}Ne state was computed as follows. First we adjusted slightly the potential depth (to $V=49$ MeV) to reproduce the actual excitation energy in ^{18}Ne [2]. Then we computed the single-particle width $\Gamma^{SP}=240$ keV, as described in the Appendix, and multiplied Γ^{SP} by the ^{17}O(d,p) ^{18}O spectroscopic factor to obtain a predicted width of 84 ± 22 keV. This is not too different from the observed width of the the *lower* member of the doublet, $\Gamma=45\pm5$ keV, but much larger than the $\leqslant15$ keV width of the upper member. In fact, the observed width of the lower level implies a spectroscopic factor $S=0.23\pm0.02$ that is not inconsistent (considering the realistic uncertainties in extracting spectroscopic factors) with the ^{17}O(d,p) value [24].

The expected Coulomb energy shift and width of the 3^- state were calculated for two configurations: $(d_{5/2})^3(p_{1/2})^{-1}$ with a $p_{1/2}$ decay and $d_{5/2}f_{7/2}$ with a $f_{7/2}$ decay. This calculation yielded $E_x\approx5.09$ MeV and $\Gamma\leqslant2$ keV. The estimated width agrees with the observed width $\Gamma\leqslant15$ keV of the *higher* member of the doublet.

If we were to reverse the spin assignments of the doublet to those of Wiescher *et al.* and Funck *et al.*, we would predict $\Gamma(5.106$ MeV$)\approx1$ keV and $\Gamma(5.153$ MeV$)\approx50$ keV, in

TABLE VI. Spin assignments for ^{18}O and ^{18}Ne levels with $E_x = 4$–7 MeV.

^{18}O		^{18}Ne					
		This work		Wiescher *et al.* [a]		Funck *et al.* [b]	
J^π	E_x	J^π	E_x	J^π	E_x	J^π	E_x
1^-	4.456	1^-	4.520	1^-	4.520	1^-	4.520
3^-	5.098	3^+	4.561	3^+	4.33[c]		
2^+	5.255	0^+	4.589	0^+	4.590	0^+	4.590
0^+	5.336	2^+	5.106	(3^-)	5.090	(3^-)	5.090
3^+	5.378	3^-	5.153	(2^+)	5.146	(2^+)	5.146
2^-	5.530	2^-	5.454	2^-	5.453	2^-	5.453
1^-	6.198	(1^-)	6.15	(1^-)	6.125[c]		
(2^-)	6.351	(3^-)	6.286	(4^+)	6.294	(1^-)	6.294
3^-	6.404	(2^-)	6.345	(3^-)	6.353	(3^-)	6.353

[a]From Ref. [4].
[b]From Ref. [5].
[c]Theoretical calculations.

sharp disagreement the observed widths. This strongly suggests that the correct assignments are $J^\pi(5.106)=2^+$ and $J^\pi(5.153)=3^-$.

C. 5.45-MeV level

The 5.45-MeV level was observed in both the ^{16}O$(^3$He,$n)$ ^{18}Ne and ^{12}C$(^{12}$C,^{6}He$)$ ^{18}Ne reactions with angular distributions characteristic of an unnatural-parity state, with very weak population at forward angles. This state is not seen in ^{20}Ne(p,t) ^{18}Ne at the most forward angles, and is very weakly populated at $\theta_{lab}=11°$ (see Fig. 10). The angular distributions of the 5.45-MeV level in these three reactions, together with the Coulomb energy shift calculation and the fact that all other ^{18}Ne analogs of ^{18}O levels between $5.0\leqslant E_x\leqslant6.0$ MeV have now been identified, strongly suggest a spin assignment of $J^\pi=2^-$.

D. 6.0−7.0-MeV energy region

A previously unobserved level at $E_x=6.15$ MeV was observed in both the ^{12}C$(^{12}$C,^{6}He$)$ ^{18}Ne and ^{16}O$(^3$He,$n)$ ^{18}Ne experiments. A doublet at $E_x=6.286\pm0.010$ MeV and $E_x=6.345\pm0.010$ MeV, consistent with the earlier results of Nero, Adelberger, and Dietrich [25], was observed in the ^{16}O$(^3$He,$n)$, ^{18}Ne(p,t), and (unresolved) in the ^{12}C$(^{12}$C, ^{6}He$)$ studies. Table VI lists our proposed spin assignments for these states, as well as those assumed by Wiescher *et al.* [4] and by Funck *et al.* [5].

The well-studied mirror nucleus ^{18}O has only three known levels $J^\pi = 1^-$, (2^-), and 3^- in this excitation energy range. Our Coulomb shift calculations and the calculations of Wiescher *et al.* both indicate that the ^{18}Ne analog of the 1^- 6.20-MeV level in ^{18}O is expected to lie at $E_x\approx6.15$ MeV. The ^{18}Ne level observed at this energy has an ^{16}O$(^3$He,$n)$ angular distribution consistent with $L\leqslant2$ as shown in Fig. 5. Using the procedure described in the previous section, its width was predicted to be ≈1 keV, which is consistent with our observed value of $\Gamma\leqslant40$ keV. The strong population of this state in the ^{16}O$(^3$He,$n)$ ^{18}Ne reaction sug-

gests it has natural parity, which eliminates the possibility of $J^\pi = 2^-$.

Because we have identified the $J^\pi = 1^-$ level in ^{18}Ne at $E_x = 6.15$ MeV, the 6.3-MeV doublet in ^{18}Ne must contain the remaining $J^\pi = 3^-$ and $J^\pi = (2^-)$ states. The ^{16}O(^{3}He, n) and ^{20}Ne(p,t) both preferentially populate natural-parity states, but unnatural-parity levels can be weakly populated via complicated multistep processes. The ^{20}Ne(p,t)^{18}Ne spectrum in Fig. 10 shows that the 6.286-MeV level is populated much more strongly than the 6.345-MeV level. The ^{12}C(^{12}C,^{6}He)^{18}Ne results are also consistent with these (p,t) data; although we could not resolve the 6.30/6.35 doublet in the heavy-ion reaction, we consistently obtained better fits to other observed peaks with the assumption that the peak of the doublet was at 6.30 MeV rather than 6.35 MeV or the averaged value of 6.325 MeV. Therefore, we suggest the 6.286-MeV state has $J^\pi = 3^-$ and the remaining state at $E_x = 6.345$ MeV has $J^\pi = (2^-)$. These assignments differ from those of Wiescher *et al.* [4] who did not have the (p,t) data and had to rely on their Thomas-Ehrman shift calculations.

E. Excitation energy region above 7.0 MeV

Along with the previously observed levels at 7.06 MeV, 7.71 MeV, 7.92 MeV, 7.95 MeV, 8.10 MeV, 8.50 MeV, and 9.20 MeV (see Fig. 1), we found new levels at 7.12 MeV, 7.35 MeV, 7.62 MeV, 8.30 MeV (8.45 MeV), 8.55 MeV, 8.94 MeV, and 9.58 MeV (Fig. 12). These new levels help considerably in completing the spectrum of high excitation energy states in ^{18}Ne compared to those in ^{18}O. However, definite spins for these new states could not be determined.

Our Coulomb shift calculation predicted that the analog of the ^{18}O 4^+ level at 7.11 MeV should lie at ≈ 7.05 MeV in ^{18}Ne. We observed a single peak at $E_x = 7.07$ MeV in the ^{16}O(^{3}He,n)^{18}Ne experiment, but we obtain a better fit to this peak assuming two states at $E_x = 7.05$ MeV and $E_x = 7.12$ MeV. The combination of our ^{12}C(^{12}C,^{6}He)^{18}Ne data and a previous ^{20}Ne(p,t)^{18}Ne experiment [25] is consistent with two levels at $E_x = 7.05$ MeV and $E_x = 7.12$ MeV. The isospin mirror of the ^{18}O(7.11 MeV, $J^\pi = 4^+$) state is most probably one of these two states. For the purpose of calculating the ^{14}O(α,p) rate, we assumed that the $J^\pi = 4^+$ level is at 7.05 MeV; changing this energy to 7.12 MeV had an insignificant effect on the predicted rate over the temperature range appropriate for novas and supernovas. We also suggest $J^\pi = 1^-$ for the 7.35-MeV level (the mirror of the 7.62-MeV level in ^{18}O) based on the angular distribution shown in Fig. 5.

VI. ^{14}O(α,p)^{17}F REACTION

A. Introduction

The transformation of the hot CNO cycle nuclei into nuclei with $Z \geq 10$ is only possible via α-induced reactions on ^{14}O and ^{15}O [1,26]. It is therefore important to determine the ^{14}O(α,p)^{17}F and ^{15}O(α,γ)^{19}Ne reaction rates that link the hot CNO cycle to the rp process. Magnus *et al.* [27] calculated the ^{15}O(α,γ)^{19}Ne reaction rate using their measurements of the spectroscopic properties of low-lying ^{15}O+α resonances. They found contributions of individual reso-

nances that differed by up to a factor of 25 from earlier estimates [28]. For temperatures $0.5 \leq T_9 \leq 2.0$ ($T_9 = 1$ denotes 10^9 K), their rate showed an overall decrease compared to the previous estimate of Langanke *et al.* [29].

In very hot environments, the ^{14}O(α,p)^{17}F reaction may compete with ^{15}O(α,γ)^{19}Ne. [The ^{14}O(α,γ)^{18}Ne rate is expected to be several orders of magnitude slower than the ^{14}O(α,p)^{17}F rate at astrophysically interesting temperatures because the outgoing protons in ^{14}O(α,p) are not strongly suppressed by the Coulomb barrier.] Predictions of the ^{14}O(α,p)^{17}F reaction rate by Wiescher *et al.* [4] and by Funck *et al.* [5] have recently appeared. These disagree for temperatures $T_9 \lesssim 0.3$, largely because Funck *et al.* included the contribution of the 5.15-MeV level in ^{18}Ne which, as it is only ~ 40 keV above the ^{14}O+α threshold, increased their reaction rate by up to three orders of magnitude for temperatures $T_9 \lesssim 0.3$. However, as explained in Sec. V B the spin assignment of Funck *et al.* for the 5.15-MeV level is inconsistent with our experimental results. In the following section, we have therefore combined our new information about the ^{18}Ne level scheme together with the direct-reaction calculations of Funck *et al.* [5] to make an improved calculation of the ^{14}O(α,p)^{17}F reaction rate for temperatures up to $T_9 = 1$.

B. Calculation of the reaction rate

1. General framework

Funck *et al.* [5] found that direct-reaction contributions to the $\ell = 1$ partial wave are comparable to or even greater than the resonant contributions at certain temperatures. We therefore computed the ^{14}O(α,p)^{17}F reaction rate under the assumption that the reaction proceeds via a combination of compound-nuclear resonances and direct reactions plus the interference between these two mechanisms. The interference between the direct-reaction $\ell = 1$ partial wave and the 6.15-MeV (1^-) excited state was included by using the expression [30]

$$S(E) = S_{\text{res}}(E) + S_{\text{DR}}(E)$$
$$\pm 2(S_{\text{res}}S_{\text{DR}})^{1/2}\cos\left[\tan^{-1}\left(\frac{\Gamma(E)}{2(E-E_r)}\right)\right]. \quad (1)$$

Interference of the 7.35-MeV (1^-) state and the $\ell = 1$ direct-reaction background and interference of the 6.29-MeV (3^-) state and the $\ell = 3$ direct-reaction background do not have a significant effect on $S(E)$ and were not included in the rate calculations described in Sec. VI B 2, below. The 7.35-MeV (1^-) state has an order of magnitude smaller strength $[S_{\text{res}}(E_r)]$, a narrower width (12 vs 20 keV), and a higher energy than the 6.15-MeV level, all of which reduce the importance of the interference term involving the 7.35-MeV state. In the energy range of interest, $T_9 = 1 \Rightarrow E_0 = 1.13$ MeV (with $\triangle E_0 = \pm 0.36$ MeV), the 7.35-MeV interference term is never more than $\approx 4 \times 10^4$ MeV b, at least an order of magnitude smaller than the 6.15-MeV interference term. Interference of the 6.29-MeV (3^-) resonance is an order of magnitude weaker than the 6.15-MeV state, while the $\ell = 3$ direct-reaction background is an order of magnitude smaller than the $\ell = 1$ background as well.

TABLE VII. Predicted ^{14}O$+\alpha$ resonance parameters based on known properties of corresponding ^{18}O states.

E_x (MeV)	E_0 (MeV)	J^π	C^2S_α[a]	Γ_α (keV)	C^2S_p[b]	Γ_p (keV)	$\Gamma^{\text{expt.}}$ (keV)	$\omega\gamma(\alpha,p)$ (MeV)
5.153	0.039	3^-	0.023	4.3×10^{-55}[c]	0.03	1.7	$\leqslant15$	3.0×10^{-57}
6.150	1.036	1^-	0.023	2.2×10^{-3}	0.03	20	$\leqslant40$	6.6×10^{-6}
6.286	1.172	3^-	0.019	3.4×10^{-4}	0.03	25	$\leqslant20$	2.4×10^{-6}
7.05	1.94	4^+	0.11	4.8×10^{-2}	0.13	53	$\leqslant120$	4.3×10^{-4}
7.35	2.24	1^-	0.01[d]	1.7	0.01[d]	12	$\leqslant50$	4.5×10^{-3}

[a]From Ref. [31] unless otherwise noted.

[b]From Ref. [24] unless otherwise noted. Assumed $C^2S_p=0.01$ for the channels not observed in the ^{17}O (d,p) reaction.

[c]Because BIND cannot accurately calculate widths of states lying barely above threshold, the width of this level was computed using Eq. (5). For this resonance to have an appreciable affect on the cross section its width would have to be increased by four orders of of magnitude.

[d]Assumed value taken from Ref. [4].

Wiescher *et al.* [4] calculated the contribution to the ^{14}O$(\alpha,p)^{17}$F rate from direct ^{14}O$(\alpha,\gamma)^{18}$Ne capture to proton-unbound states and found that these processes play only a minor role. We omitted this mechanism in our calculation.

The resonant reaction cross section was assumed to have a Breit-Wigner form

$$\sigma(E) = \pi\lambdabar^2 \sum_i \frac{2J_i+1}{(2J_T+1)(2J_P+1)} \frac{\Gamma_\alpha^i(E)\Gamma_p^i(E)}{(E-E_R^i)^2+[\Gamma_i(E)/2]^2}. \tag{2}$$

Because both the target and the projectile have $J^\pi=0^+$ ground states, the sum on i runs over natural-parity levels of ^{18}Ne. The energy dependence of the widths was taken into account by letting the partial widths Γ_α and Γ_p vary as

$$\Gamma_x^i(E) = \Gamma_x^i(E_R^i)\frac{P_\ell(E)}{P_\ell(E_R^i)}, \tag{3}$$

where the P_ℓ are Coulomb penetrabilities calculated at radii of 4.99 fm and 4.47 fm for the α and p channels, respectively.

The partial widths $\Gamma_\alpha(E_R)$ and $\Gamma_p(E_R)$ are not known directly, and had to be inferred from the mirror nucleus ^{18}O using isospin symmetry. They were obtained from the expression

$$\Gamma_x^i(E_R^i) = C^2S_i\Gamma_x^{i,\text{SP}}, \tag{4}$$

where the proton and alpha spectroscopic factors S_i were taken from ^{17}O(d,p) [24] and ^{14}C$(^6$Li$,d)$ [31] transfer-reaction data. The ^{18}Ne single-particle widths $\Gamma_x^{i,\text{SP}}$ were computed in two ways

(1) Using a Woods-Saxon code as discussed in Sec. V B above and in the Appendix. For consistency, we took the geometry of the ^{14}O$+\alpha$ potential ($R=R_c=5.00$ fm, $a=0.65$ fm) to be identical to the ^{14}C$+\alpha$ potential used in the DWBA analysis of the ^{14}C$(^6$Li$,d)$ data [31]; the number of nodes in the $\alpha+^{14}$O wave function was taken from the harmonic-oscillator model assuming the particles to be in the lowest available shell-model orbits. The geometry of the

^{17}F$+p$ potential ($R=R_c=3.21$ fm, $a=0.65$ fm) was identical to the ^{17}O$+p$ potential used in the DWBA analysis of the ^{17}O(d,p) data [24].

(2) Using the simple expression

$$\Gamma^{\text{SP}}(E_r) = 3\frac{\hbar^2}{\mu R^2}P_\ell(E_r), \tag{5}$$

where the alpha and proton penetrabilities were calculated at radii of 4.99 fm, and 4.47 fm respectively.

The results from these two procedures agreed reasonably well, typically within a factor of 3 and within a factor of 5 for the worst case. We adopt and tabulate the widths obtained from the Woods-Saxon approach as these were based on a consistent approach for relating transfer-reaction cross sections to the widths of levels in the mirror nucleus. The predicted partial alpha and proton widths of the lowest ^{14}O$(\alpha,p)^{17}$F resonances are listed in Table VII.

We have restricted our calculations to temperatures below $T_9=1$, relevant for nova explosions and some x-ray bursts and supernovas. At these temperatures, the compound nuclear contributions to these reaction rates are dominated by resonances in the region we studied in this work.

2. Results and astrophysical implications

Funck *et al.* [5] predicted a strong contribution to the $\ell=2$ partial wave of S_{total} that arose almost entirely from the 5.15-MeV state. We have shown that this state is much more likely to have $J^\pi=3^-$, which greatly reduces the $\ell=2$ contribution. Because of the much narrower width of the 3^- state, its tail has a much smaller influence on S_{total}.

Figure 13 shows the $S_{\text{total}}(E)$ resulting from the summed resonant contributions of the 5.153-MeV ($J^\pi=3^-$), 6.15-MeV ($J^\pi=1^-$), 6.286-MeV ($J^\pi=3^-$), 7.05-MeV ($J^\pi=4^+$), and 7.35-MeV ($J^\pi=1^-$) states, together with the direct $\ell=1$ contribution and its interference with the 6.15-MeV resonance, in comparison with the previous calculations of Funck *et al.* [5]. The figure shows that our new information about the resonances (especially, the 6.15-MeV resonance) make significant contributions to the ^{14}O$(\alpha,p)^{17}$F reaction rate.
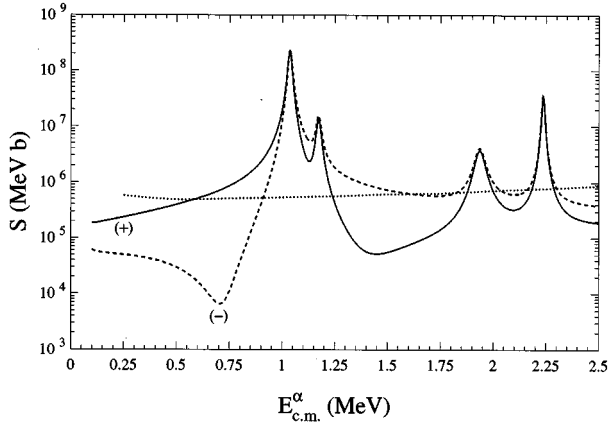
$$N_A\langle\sigma v\rangle=1.54\times10^{11}(AT_9)^{-3/2}\sum_i \omega\gamma_i\exp\left(-11.605\frac{E_i}{T_9}\right),\tag{7}$$

which for the ^{14}O(α,p) ^{17}F reaction for the 5.153-, 6.286-, 7.05-, and 7.35-MeV states, respectively, becomes

$$\begin{aligned}N_A\langle\sigma v\rangle=&8.42\times10^{-47}(T_9)^{-3/2}\exp(-0.453/T_9)\\&+6.74\times10^4(T_9)^{-3/2}\exp(-13.60/T_9)\\&+1.21\times10^7(T_9)^{-3/2}\exp(-22.51/T_9)\\&+1.26\times10^8(T_9)^{-3/2}\exp(-26.00/T_9).\tag{8}\end{aligned}$$

The integral in Eq. (6) for the 6.15-MeV state, the $\ell=1$ direct-reaction background, and their associated interference was evaluated numerically and then added to the expression for the other four resonances. The resulting $N_A\langle\sigma v\rangle$ values are presented as a function of T_9 in Table VIII and in Fig. 14. For all the temperatures in the range $T_9<1$, the 6.15-MeV state, the $\ell=1$ direct-reaction background, and their interference account for more that 92% of the total reaction rate; for $T_9<0.5$, appropriate for all nova explosions, they account for more than 98% of the total reaction rate.

For comparison, the calculated ^{14}O(α,γ) ^{18}Ne reaction rate [4] and the ^{15}O(α,γ) ^{19}Ne reaction rate based on the recently revised estimate of the strength for the lowest (unmeasured) resonance $\omega\gamma=20\mu$eV [32] are also plotted in Fig. 14. While both the ^{14}O(α,p) and ^{15}O(α,γ) reactions may serve to initiate breakout paths from the hot CNO cycle, our results indicate that ^{15}O(α,γ) is significantly faster than

FIG. 13. The ^{14}O(α,p) S factor predicted from the partial widths in Table VII. The solid and dashed lines show S_{total} for the two choices of the sign of the interference between the direct process and the 1.036-MeV resonance; the dotted line shows the S factor from the previous work of Funck, Grund, and Langanke [5], which did not include contributions from the new resonances found in this work. The figure shows that our new information about the resonances (especially, the 6.15-MeV resonance) makes significant contributions to the ^{14}O(α,p) ^{17}F reaction rate.

The reaction rate, expressed in terms of $S(E)$, is given by

$$N_A\langle\sigma v\rangle=N_A\left(\frac{8}{\pi\mu(kT)^3}\right)^{1/2}\int_0^\infty S(E)\exp\left(-\frac{E}{kT}-\frac{E_G^{1/2}}{E^{1/2}}\right)dE.\tag{6}$$

For isolated resonances this reduces to

TABLE VIII. Reaction rates.

T_9	^{14}O(α,p) [a] (cm^3 mol^{-1} s^{-1})	^{14}O(α,p) [b] (cm^3 mol^{-1} s^{-1})	^{14}O(α,γ) [c] (cm^3 mol^{-1} s^{-1})	^{15}O(α,γ) [d] (cm^3 mol^{-1} s^{-1})
0.10	2.07×10^{-21}	4.34×10^{-22}	4.19×10^{-51}	7.03×10^{-25}
0.15	8.44×10^{-17}	1.37×10^{-17}	2.18×10^{-34}	1.12×10^{-16}
0.20	7.15×10^{-14}	8.66×10^{-15}	4.38×10^{-26}	1.25×10^{-12}
0.25	9.03×10^{-12}	7.78×10^{-13}	3.89×10^{-21}	3.10×10^{-10}
0.30	3.85×10^{-10}	2.72×10^{-11}	7.38×10^{-18}	1.17×10^{-8}
0.35	9.16×10^{-9}	1.44×10^{-9}	1.56×10^{-15}	1.51×10^{-7}
0.40	1.70×10^{-7}	6.71×10^{-8}	8.43×10^{-14}	1.01×10^{-6}
0.45	2.43×10^{-6}	1.51×10^{-6}	1.84×10^{-12}	4.42×10^{-6}
0.50	2.42×10^{-5}	1.84×10^{-5}	2.13×10^{-11}	1.46×10^{-5}
0.55	1.69×10^{-4}	1.42×10^{-4}	1.56×10^{-10}	4.03×10^{-5}
0.60	8.68×10^{-4}	7.72×10^{-4}	8.08×10^{-10}	1.01×10^{-4}
0.65	3.49×10^{-3}	3.22×10^{-3}	3.23×10^{-9}	2.40×10^{-4}
0.70	1.15×10^{-2}	1.09×10^{-2}	1.05×10^{-8}	5.56×10^{-4}
0.75	3.23×10^{-2}	3.14×10^{-2}	2.90×10^{-8}	1.24×10^{-3}
0.80	7.93×10^{-2}	7.86×10^{-2}	7.03×10^{-8}	2.65×10^{-3}
0.85	1.75×10^{-1}	1.76×10^{-1}	1.53×10^{-7}	5.39×10^{-3}
0.90	3.52×10^{-1}	3.61×10^{-1}	3.05×10^{-7}	1.03×10^{-2}
0.95	6.58×10^{-1}	6.83×10^{-1}	5.65×10^{-7}	1.87×10^{-2}
1.00	1.15	1.21	9.86×10^{-7}	3.22×10^{-2}

[a]Assuming constructive interference below the 1.036-MeV resonance.
[b]Assuming destructive interference below the 1.036-MeV resonance.
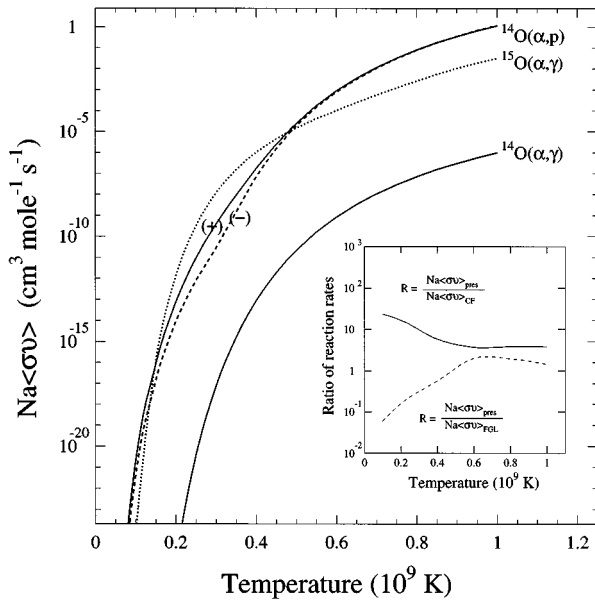[c]From Ref. [4].
[d]From Ref. [32].

FIG. 14. The ^{14}O(α,p) ^{17}F reaction rate as a function of temperature. The solid line and dashed lines correspond to the two possible signs of the interference of the 1.036-MeV resonance and direct reactions. The dotted line is the competing ^{15}O(α,γ) reaction rate from Ref. [32]. The ^{14}O(α,γ) reaction rate from Ref. [4] is also plotted. The inset shows a comparison of the present ^{14}O(α,p) ^{17}F rate with the previous rates of Caughlan and Fowler [33] (solid line) and Funck *et al.* [5] (dotted line).

^{14}O(α,p) at temperatures below $T_9 \sim 0.48$ (covering the expected range for nova explosions) and will therefore dominate the breakout from the hot CNO cycle into the rp process. However, in higher-temperature explosions (such as x-ray bursts associated with accreting neutron stars), the ^{14}O(α,p) reaction will dominate. It is also clear that ^{14}O(α,γ) does not compete significantly with ^{14}O(α,p) anywhere in this entire temperature range.

Some words of caution are in order. The low-temperature rates for both the ^{14}O(α,p) and the ^{15}O(α,γ) reactions depend, in each case, almost entirely on a single resonance where the important widths that determine the resonance strength, $\omega\gamma$, had to be extracted from indirect measurements. Furthermore, at temperatures above $T_9 \sim 1.5$, the ^{14}O(α,p) reaction rate contains very significant contributions from resonances, about which very little is known beyond their energies.

VII. CONCLUSIONS

Our revised spin assignments for the 5.11- and 5.15-MeV levels of ^{18}Ne, $J^\pi = 2^+$, and $J^\pi = 3^-$, respectively, lower the ^{14}O(α,p) ^{17}F reaction rate calculated by Funck *et al.* [5] by up to three orders of magnitude at temperatures $T_9 \lesssim 0.3$. Our discovery of new ^{18}Ne levels at $E_x = 6.15 \pm 0.01$ MeV, 7.12 ± 0.02 MeV, 7.35 ± 0.02 MeV, 7.62 ± 0.02 MeV, 8.30 ± 0.02 MeV (8.45 ± 0.03 MeV), 8.55 ± 0.03 MeV, 8.94 ± 0.02 MeV, and 9.58 ± 0.02 MeV allowed us to find ^{18}Ne analogs for all ^{18}O states up to $E_x = 7.5$ MeV. Armed with information about these new levels, we have computed a rate for the ^{14}O(α,p) ^{17}F reaction for $T_9 \lesssim 1$ that is on much firmer experimental grounds than previous calculations.

APPENDIX

Because our experiments determined only the *total* widths of the ^{18}Ne levels, the *partial* widths for the α and p decay channels had to be inferred from known α and n spectroscopic factors of the corresponding levels in the mirror nucleus ^{18}O. This required identifying probable isobaric correspondences, based on measured spectroscopic properties and on the expected Coulomb energy shifts between ^{18}Ne and ^{18}O. The shifts were calculated as explained in Sec. V B using a standard Woods-Saxon program BIND [7].

We also needed the single-particle α and p widths for the ^{18}Ne levels. We encountered a problem in computing level widths when the particle decay was not substantially inhibited by the barrier. Optical model codes conventionally compute Γ^{SP} using the expression

$$\Gamma^{SP} = 2[d\delta_\ell/dE(\delta_\ell = 90°)]^{-1}. \quad \text{(A1)}$$

This yields widths that are too large for very broad resonances where the energy dependence of the width is not negligible. We therefore deduced the single-particle width from the full width at half maximum (FWHM) of the $\widetilde{S}$ factor, defined by

$$\widetilde{S} = \frac{\sigma E}{P_\ell^2}, \quad \text{(A2)}$$

where P_ℓ is the Coulomb penetrability and σ is the cross section,

$$\sigma = \frac{4\pi}{k^2}(2l+1)\sin^2\delta_\ell, \quad \text{(A3)}$$

calculated from the phase shift $\delta_\ell(E)$ predicted by BIND; this procedure is also valid for a narrow resonance.

The results of our Woods-Saxon calculations are shown in Table IX, where $E_n = E_x - E(\text{threshold})$ denotes the energy of the neutron orbiting around ^{17}O and V the depth of the strong potential well that produces a stationary state with energy E_n. E_p is the corresponding energy of a proton orbiting around ^{17}F in the same strong potential plus a Coulomb term; Δ^{SP} would be the Coulomb energy if the level had the pure single-particle configuration specified in the fourth column. The column "C^2S" gives the spectroscopic factors from Ref. [24] that were used to predict the excitation energies and widths of the ^{18}Ne levels listed in columns 9 and 10.

TABLE IX. Coulomb shifts calculated using the code BIND.

	Measured								Calculated		Measured	
J^π	$E_x(^{18}O)$	$E_n(^{18}O)$	Decay[a]	V	$E_p(^{18}Ne)$	Δ	Γ_{sp} (keV)[b]	C^2S[c]	$E_x^*(^{18}Ne)$[d]	Γ^* (keV)[e]	$E_x(^{18}Ne)$	Γ (keV)
0^+	0.00	-8.04	$d_{5/2}$	69.7	-3.82	0.10		1.22	0.12	bnd	0.00	bnd
2^+	1.98	-6.06	$d_{5/2}$	60.2	-1.96	-0.02	bnd	0.83				
2^+	1.98	-6.06	$s_{1/2}$	55.5	-2.24	-0.30	bnd	0.21	1.82	bnd	1.89	bnd
4^+	3.55	-4.49	$d_{5/2}$	46.9	-0.60	-0.23	bnd	1.57	3.19	bnd	3.38	bnd
0^+	3.63	-4.41	$d_{5/2}$	62.3	-0.37	-0.08	bnd	0.28	3.61	bnd	3.58	bnd
2^+	3.92	-4.12	$s_{1/2}$	50.8	-0.53	-0.53	bnd	0.35	3.72	bnd	3.62	bnd
1^-	4.46	-6.63^f	$s_{1/2}^{\ f}$	59.0	-2.74	-0.18	bnd	h				
1^-	4.46	-6.63^f	$d_{5/2}^{\ f}$	64.9	-2.50^f	0.06	bnd	h	4.46	bnd	4.52	9 ± 6
3^-	5.10	-2.94	$p_{1/2}$	25.5	$+0.80$	-0.38	85	0.02				
3^-	5.10	-2.94	$f_{7/2}$	87.1	$+0.98$	-0.20	1	0.03				
3^-	5.10	-6.00^f	$d_{5/2}^{\ f}$	55.0	-1.97^f	-0.05	bnd	h	5.09	1.7	5.15	≤15
2^+	5.25	-2.79	$s_{1/2}$	47.5	$+0.50$	-0.83	353	0.35	4.96	125	5.10	45 ± 5
0^+	5.34	-2.70	$d_{5/2}$	58.5	$+1.19$	-0.23	0.3	0.16				
0^+	5.34	-3.57^g	$s_{1/2}^{\ g}$	53.1	-0.06^g	-0.98	≤0.1	h	5.29	≤0.1	4.59	4 ± 4
3^+	5.37	-2.67	$s_{1/2}$	44.1	$+0.59$	-0.86	27	1.0	4.51	27	4.56	?
2^-	5.53	-5.56^f	$d_{5/2}^{\ f}$	59.0	-1.48	$+0.01$	bnd	h	5.53	bnd^f	5.45	≤20
1^-	6.20	-1.84	$p_{3/2}$	26.7	$+1.70$	-0.58	660	0.03				
1^-	6.20	-4.89^f	$s_{1/2}^{\ f}$	55.1	-1.19	-0.35	bnd	h				
1^-	6.20	-4.89^f	$d_{5/2}$	61.4	-0.86	-0.04	bnd	h	6.18	20	(6.15)	(≤40)
3^-	6.40	-1.64	$p_{1/2}$	22.9	$+1.79$	-0.69	830	0.03	6.38	25	(6.29)	(≤20)
4^+	7.12	-0.92	$d_{3/2}$	40.1	$+2.57$	-0.73	400	0.13	7.04	53	(7.05)	(≤120)
1^-	7.62	-0.42	$p_{1/2}$	23.1	$+3.07$	-0.63	1200	h	7.61	12	(7.35)	(≤50)

[a]To the ground state unless otherwise noted.

[b]Single-particle widths estimated by modifying the potential depth V until we obtained an energy in agreement with the experimental value, and according to the method described in the Appendix.

[c]From Ref. [24] unless otherwise noted.

[d]Expected E_x in ^{18}Ne taking into account the spectroscopic factor.

[e]This width was estimated as the sum of products of the single-particle widths in column 8 times the C^2S's.

[f]With respect to $^{17}O(1/2^-)+n$ or $^{17}F(1/2^-)+p$.

[g]With respect to $^{17}O(1/2^+)+n$ or $^{17}F(1/2^+)+p$.

[h]C^2S not known, assumed $=0.01$.

Our predicted Coulomb shifts $\Delta = E_x(^{18}Ne) - E_x(^{18}O)$ were related to the single-particle Coulomb shifts by

$$\Delta = \sum_i S_i^* \Delta_i^{SP}. \qquad (A4)$$

For particles in different configurations, such as $s_{1/2}$, or $d_{5/2}$, S^* is just the spectroscopic factor. However, for particles in identical configurations where $S=2$, such as $d_{5/2}^2$ or $s_{1/2}^2$ we set $S^*=S/2$ because the Coulomb shift due to one of the particles was already taken into account when we calculated excitation energies with respect to the appropriate $n + ^{17}O$ or $p + ^{17}F$ thresholds, as the $A=17$ states contain the Coulomb shift of one particle.

The level widths were estimated as

$$\Gamma^* = \sum_i S_i \Gamma_i^{SP}, \qquad (A5)$$

where the sum was taken over all possible configurations, S_i denotes the spectroscopic factor, and Γ_i^{SP} denotes the single-particle width computed as described above. For configurations with two particles in the same orbit, such as $d_{5/2}^2$ or $s_{1/2}^2$ the spectroscopic factor of 2 accounts for the fact that either particle 1 leaves particle 2 plus the ^{16}O core or vice versa.

[1] R. K. Wallace and S. E. Woosley, Astrophys. J. Suppl. Series **45**, 389 (1981).

[2] A. García, E. G. Adelberger, P. V. Magnus, D. M. Markoff, K. B. Swartz, M. S. Smith, K. I. Hahn, N. Bateman, and P. D. Parker, Phys. Rev. C **43**, 2012 (1991).

[3] M. Wiescher, J. Görres, and F.-K. Thielemann, Astrophys. J. **326**, 384 (1988).

[4] M. Wiescher, V. Harms, J. Görres, F.-K. Thielemann, and L. J.

Rybarcyk, Astrophys. J. **316**, 162 (1987).

[5] C. Funck, B. Grund, and K. Langanke, Z. Phys. A **332**, 109 (1989); C. Funck and K. Langanke, Nucl. Phys. **A480**, 188 (1988).

[6] F. Ajzenberg-Selove, Nucl. Phys. **A475**, 1 (1987).

[7] A. García, Ph.D. thesis, University of Washington, 1991.

[8] P. B. Fernández, E. G. Adelberger, and A. García, Phys. Rev. C **40**, 1887 (1989).

[9] R. R. Borchers and C. H. Poppe, Phys. Rev. C **129**, 2679 (1963).

[10] S. A. Elbakr, I. J. Van Heerden, W. J. McDonald, and G. C. Neilson, Nucl. Instrum. Methods **105**, 519 (1972).

[11] M. S. Smith, A. W. Wright Nuclear Structure Laboratory Progress Report, Yale University, 1987–1988 (unpublished).

[12] P. D. Kunz and E. Rost (private communication).

[13] E. G. Adelberger and A. B. McDonald, Nucl. Phys. **A145**, 497 (1970).

[14] K. I. Hahn, Ph.D. thesis, Yale University, 1993.

[15] H. Feshbach, in *Nuclear Spectroscopy*, edited by F. Ajzenberg-Selove (Academic Press, New York, 1960).

[16] R. G. Stokstad, Wright Nuclear Structure Laboratory Internal Report No. 52, Yale University, 1972 (unpublished).

[17] D. Shapira, R. G. Stokstad, and D. A. Bromley, Phys. Rev. C **10**, 1063 (1974).

[18] C. M. Perey and F. G. Perey, At. Data Nucl. Data Tables **17**, 1 (1976).

[19] M. S. Smith, P. V. Magnus, K. I. Hahn, A. J. Howard, P. D. Parker, A. E. Champagne, and Z. Q. Mao, Nucl. Phys. **A536**, 333 (1992); M. S. Smith, Ph.D. thesis, Yale University, 1990.

[20] A. K. Opper, Ph.D. thesis, Indiana University, 1991.

[21] E. J. Stephenson, K600 Manual (XSYS data acquisition system for the K600 spectrometer with the focal-plane polarimeter), IUCF, 1992.

[22] R. T. Kouzes, Ph.D. thesis, Princeton University, 1974.

[23] K. I. Hahn, C. R. Brune, and P. R. Wrean, Phys. Rev. C **48**, 914 (1993).

[24] T. K. Li, D. Dehnhard, R. E. Brown, and P. J. Ellis, Phys. Rev. C **13**, 55 (1976).

[25] A. V. Nero, E. G. Adelberger, and F. S. Dietrich, Phys. Rev. C **24**, 1964 (1981).

[26] M. Wiescher, J. Görres, F.-K. Thielemann, and H. Ritter, Astron. Astrophys. **160**, 56 (1986).

[27] P. V. Magnus, M. S. Smith, P. D. Parker, R. E. Azuma, C. Campbell, J. D. King, and J. Vise, Nucl. Phys. **A470**, 206 (1987); P. V. Magnus, M. S. Smith, A. J. Howard, P. D. Parker, and A. E. Champagne, *ibid.* **A506**, 332 (1990).

[28] F. Ajzenberg-Selove, Nucl. Phys. **A392**, 1 (1983).

[29] K. Langanke, M. Wiescher, W. A. Fowler, and J. Görres, Astrophys. J. **301**, 629 (1986).

[30] E.g., G. J. Mathews and F. S. Dietrich, Astrophys. J. **287**, 969 (1984).

[31] A. Cunsolo, A. Foti, G. Imme, G. Pappalardo, G. Raciti, and N. Sauier, Phys. Rev. C **24**, 476 (1981).

[32] Z. Q. Mao, H. T. Fortune, and A. G. Lacase, Phys. Rev. Lett. **74**, 3760 (1995).

[33] G. R. Caughlan and W. A. Fowler, At. Data Nucl. Data Tables **40**, 283 (1988).